Use of EBIC for MTF measurement of HOT MCT focal plane planar array with very small pixel pitches

Samantha Bustillos Vasco, Nicolas Baier, Clément Lobre, Olivier Gravrand, Laurent Rubaldo

PROCEEDINGS OF SPIE

SPIEDigitalLibrary.org/conference-proceedings-of-spie

Use of EBIC for MTF measurement of HOT MCT focal plane planar array with very small pixel pitches

S. Bustillos Vasco, N. Baier, C. Lobre, O. Gravrand, L. Rubaldo

S. Bustillos Vasco, N. Baier, C. Lobre, O. Gravrand, L. Rubaldo, "Use of EBIC for MTF measurement of HOT MCT focal plane planar array with very small pixel pitches," Proc. SPIE 12534, Infrared Technology and Applications XLIX, 1253412 (13 June 2023); doi: 10.1117/12.2663758

SPIE.

Event: SPIE Defense + Commercial Sensing, 2023, Orlando, Florida, United States

Use of EBIC for MTF measurements of HOT MCT focal plane planar array with very small pixel pitches

S. Bustillos Vasco[a], N. Baier[a], C. Lobre[a], O. Gravrand[a], L. Rubaldo[b]
[a]CEA LETI, 17 rue des martyrs, 38054 Grenoble, France
[b]LYNRED, BP21, 38113 Veurey-Voroize, France

ABSTRACT

Today, the trend line in cooled infrared detector manufacturing is to go towards very small pixel pitches and to operate at high temperatures. To take full advantage of this pitch reduction, the modulation transfer function (MTF) has to be correctly measured to optimize the development of HgCdTe p/n planar diodes, where the MTF is degraded due to the large diffusion length of minority carriers. Furthermore, as the pitch decreases close to the wavelength, the measurement of its MTF becomes difficult using traditional optical projection methods, which are intrinsically limited by diffraction. In order to assess this MTF, an original characterization method is therefore investigated at LETI, involving an electron beam instead of an optical beam to excite the pixels: the electron beam induced current (EBIC). This method introduces a low MTF degradation (estimated by Monte Carlo simulations) on the measurements that can be neglected, thus giving access to a direct estimation of the pixel MTF, with no need for deconvolution. This work shows EBIC measurements carried out on HgCdTe planar diodes with small pixel pitches: 7.5µm and 5µm. The resulting MTF is compared with MTF computed by finite-element modeling using an electronic and photonic excitation.

Keywords: EBIC, MTF, MWIR, HgCdTe, p/n technology, HOT, small pixel pitch

1. INTRODUCTION

The motivation for switching from an intrinsic Hg-doped HgCdTe (MCT) n/p technology to an extrinsic As/In-doped HgCdTe p/n technology is the increase in minority carrier lifetime in the absorbing layer and the associated decrease in dark current. On one hand, the reduction of dark current allows an increase in the operating temperature of the detectors [1]. On the other hand, this gain in lifetime means a significant increase in diffusion length of the minority carriers estimated to be greater than 20µm. In other words, the holes generated have the ability to diffuse further in the n-type absorbing layer, which makes the separation of information between pixels a challenge for the p/n technology.

Moreover, in order to increase the detection range, the reduction of the pixel pitch is a major issue for the new generation of p/n infrared detectors. For the mid-wave infrared range (MWIR) with a cut-off length of 5µm and a F#2 numerical aperture, the desired pixel pitch is estimated to be 5µm [2]. By considering a diffusion length higher than 20µm, the minority carriers have the possibility to diffuse in a radius greater than 4 pixels, thus causing a possible charge sharing between diodes resulting in a degradation of the modulation transfer function (MTF) of the pixel.

The development of MCT p/n planar diodes with small pixel pitch and a high-operability-temperature (HOT) aims at optimized structure of planar diodes to minimize the effect of the diffusion length on the MTF. Therefore, the measurement of the MTF is fundamental on the ongoing development. However, for small pixel pitches, smaller than 10µm, optical methods are no longer suitable for estimating the MTF due to the diffraction limit: the spatial response of a pixel becomes comparable to the Airy disk size.

This work focuses on the measurement of the MTF by the electron beam-induced current (EBIC) method. The advantage of this technique over optical projection methods is the resolution of the electron beam and the simplicity of focusing using a scanning electron microscope (SEM). The first section of this work details the EBIC operating principle and the characterized diode planar structure. In the results part, EBIC acquisitions are presented for two pixel pitches: 7.5µm and 5µm. For the 7.5µm pixel pitch, the MTF estimated by EBIC is compared with the one estimated using a classical optical projection method, the knife-edge method. From EBIC acquisitions, it is possible to directly estimate the pixel MTF because the degradation introduced by the experimental bench on the measurements can be neglected. To verify this, Monte Carlo simulations are performed in order to compute the interactions between the incident electrons and the MCT matter. The resulting interaction volume allows to quantify the EBIC degradation on the MTF measurements and to determine the carrier generation profile in the MCT volume. Knowing this electro-generation profile, finite element

Infrared Technology and Applications XLIX, edited by Gabor F. Fulop, David Z. Ting, Lucy L. Zheng, Proc. of SPIE Vol. 12534, 1253412 · © 2023 SPIE
0277-786X · doi: 10.1117/12.2663758

modelling (FEM) is performed to simulate the MTF and to compare with MTF measurements. Furthermore, using a classical photo-generation profile resulting from the excitation of the MCT by IR photons, the pixel MTF is simulated in order to assess the representativeness of the MTF measurements by EBIC.

2. METHOD

The EBIC technique developed at CEA-LETI for the MTF measurement was presented for the first time by A.Yèche et al. [3]. This method takes place in a scanning electron microscope and consists in recovering the current coming from a semiconductor during the scanning of its surface by an electron beam. The electron beam generates electron-hole pairs at each position in a small volume known as interaction volume [4]. These created carriers diffuse in the semiconductor until they recombine or are collected by the electric field of a p/n junction, thus giving rise to the EBIC current. In this way, an EBIC cartography is reconstructed from the signal delivered by a diode at each position of the beam. Considering the generation volume much smaller than the pixel sensitive area, the EBIC image corresponds to an estimate of the diode point spread function (PSF). The diode MTF is then determined by taking the Fourier transform of this measurement PSF.

To be consistent with the classical illumination configuration, the electron beam is injected on the backside of the device as it is illustrated in Figure 1. Contrary to IR photons, which are invisible to the substrate, electrons must be injected directly into the active layer (MCT – n doped) to create free carriers by inelastic interactions. This requires the removal of the CdZnTe (CZT) substrate for this observation setup. The thinning process to remove the substrate is carried out after the test chip is flip chipped onto a Si fan-out. Thinning technique was developed at Leti and used to characterize small pixel pitch focal plane arrays (FPA) at Leti and Lynred.

The Figure 1 shows a diagram representing the structure of planar diodes characterized in this work. The output signal comes from the central diode, illustrated in red (array diode). This diode is surrounded by two rows of identical diodes (confinement) biased together, thus representing a mini array to mimic a FPA configuration. The n doping of the active layer is done during the MCT liquid phase epitaxy (LPE) on the CZT substrate. The p region is doped by As implantation.

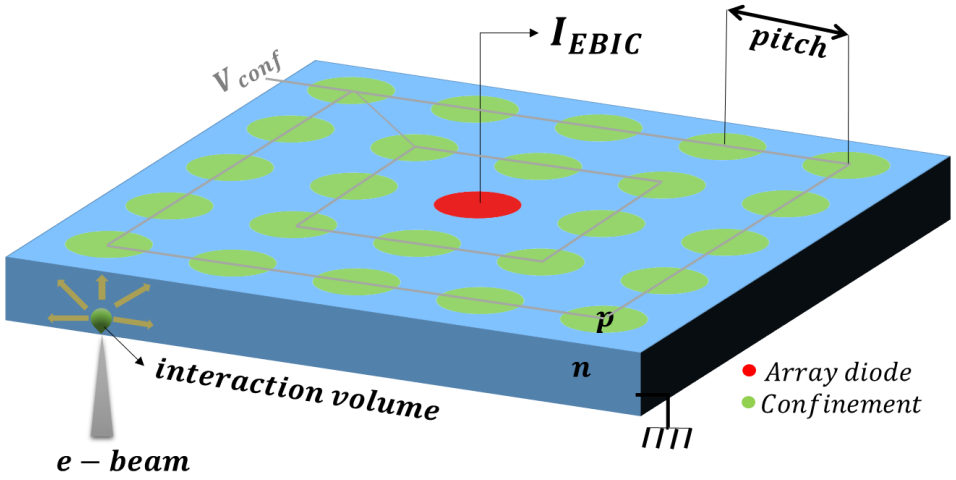

Figure 1. Illustration of the test chip and the EBIC injection configuration.

3. EXPERIMENTAL RESULTS

The EBIC mapping acquisitions shown in this section were obtained using a 15keV electron beam modulated at 10 kHz by a beam-blanker. The beam modulation allows the use of a lock-in detection to obtain only the DC component of the output signal and to filter parasitic signals: the dark current and the current of the IR radiation of the SEM at 300K. Measurements are performed at 120K thanks to a liquid nitrogen cooling circuit installed inside the SEM while keeping the chamber under vacuum.

Using EBIC, two test chips were characterized: one containing a 7.5µm pitch MCT diode array and the other containing a 5µm pitch MCT diode array. Figure 2 shows the EBIC current maps delivered by the central diodes of these two structures. The white circles were added to illustrate the neighboring diodes.

Even if the minority carriers (holes) have a long diffusion length compared to the pixel pitch, the PSF obtained brings out that the lateral diffusion is reduced. Indeed, the carriers created around the diode are pumped by the neighboring diodes, thus preventing their diffusion towards the central diode. This effect of carrier pumping by neighboring diodes is called self-confinement [5] and it is noticeable by the cloverleaf shape of the PSF.

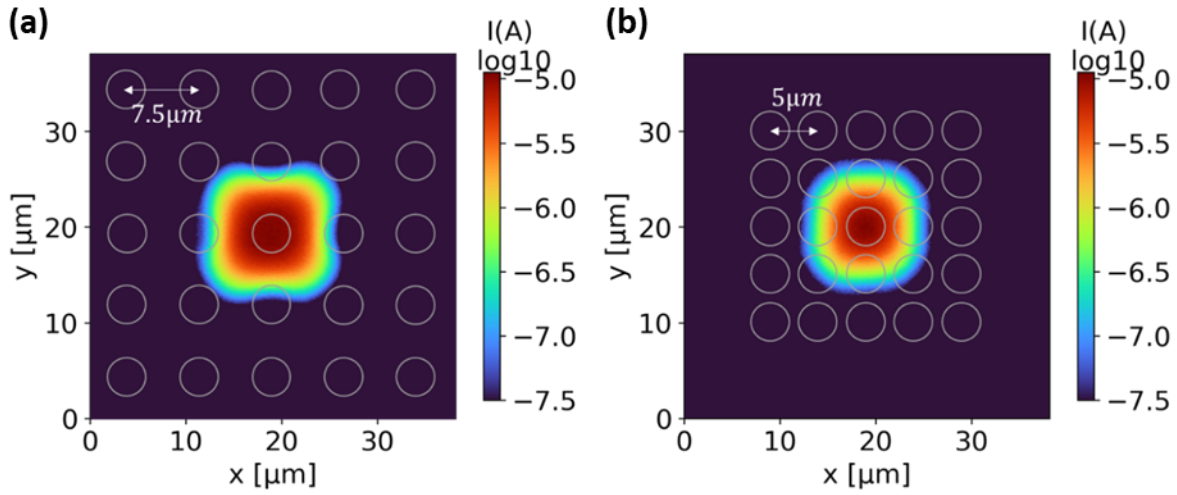

Figure 2. PSF obtained by EBIC scans of a (a) 7.5µm and (b) 5µm pitch array diodes.

This cloverleaf shape appears more pronounced for the 7.5µm pixel pitch than for the 5µm pixel pitch, highlighting a more important self-confinement effect. Figure 3 shows the line spread function (LSF) for these two pixel pitches, obtained from the integral of the PSF along one direction. These profiles are not square, due to the effect of lateral diffusion and the charge sharing between pixels. The full widths at half maximum (FWHM) are 7.41 and 5.15µm respectively, showing a gain in resolution with the reduction of the pixel size. In frequency space, the reduction of the pixel size increases the spatial bandwidth of the pixels, defined by the maximum frequency well-sampled according to the Shannon theorem: the Nyquist frequency equals to $\frac{1}{2\ pitch}$. This frequency ranges from 67 to 100mm^{-1} for pixel pitch of 7.5 and 5µm respectively.

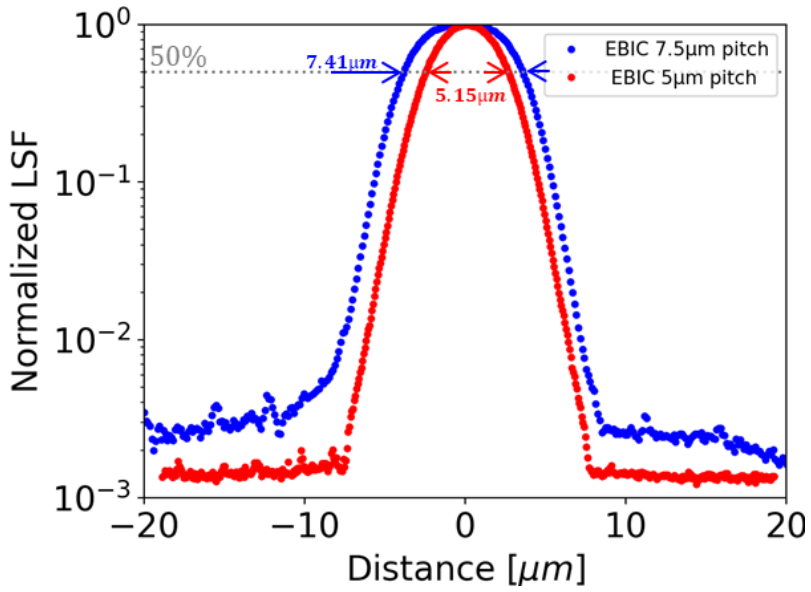

Figure 3. LSF determined from the PSF in Figure 2

The Fourier transforms of the measured PSF are plotted in Figure 4 by circles in blue for the 7.5µm and in red for the 5µm pixel pitch. The narrowing of the LSF is reflected in the Fourier space by an increase in the MTF. In fact, the MTF for the 5µm pixel pitch is higher than that of 7.5µm. On the same figure, the solid line curves show the MTF of an ideal pixel, corresponding to the Fourier transform of its square spatial response:

$$MTF_{ideal}(f) = sinc(\pi f \times pitch) \quad (1)$$

At the Nyquist frequency, the ideal MTF is 64%. In the case of MTF determined by EBIC, the MTF value at Nyquist frequency for the 7.5µm pixel pitch is equal to **52%** and **42%** for the 5µm. This shows that the 7.5µm pixel pitch structure allows a better charge separation between pixels than the 5µm pixel pitch structure. Indeed, the PSF presented previously shows a stronger self-confinement effect for the 7.5µm pitch limiting more the lateral diffusion of minority carriers. However, the MTF of the 5µm pixel pitch remains higher than the 7.5µm pixel MTF over a large range of frequency, suggesting a gain of detection range switching from 7.5µm to 5µm pitch.

The Figure 4 also shows the MTF of a 7.5µm pixel pitch FPA estimated by the deconvoluted knife-edge method [6] (blue squares) using the same diode design as the EBIC sample. This optical measurement shows a 50% MTF at Nyquist. For the same pixel pitch, MTF curves estimated by EBIC and knife-edge are then quite close to each other with only a 2% difference at Nyquist. On one side, this difference can be due to the fact that samples are different. With EBIC, a sample containing mini-arrays of bare diodes was characterized as previously explained, while for the knife-edge method, the complete focal plane array diode was measured, including a full ROIC. On the other side, the optical method needs a deconvolution to obtain the true value of pixel MTF, which can introduce uncertainties in the measurement. On the other hand, EBIC estimates a direct pixel MTF without deconvolution, as discussed in the next section.

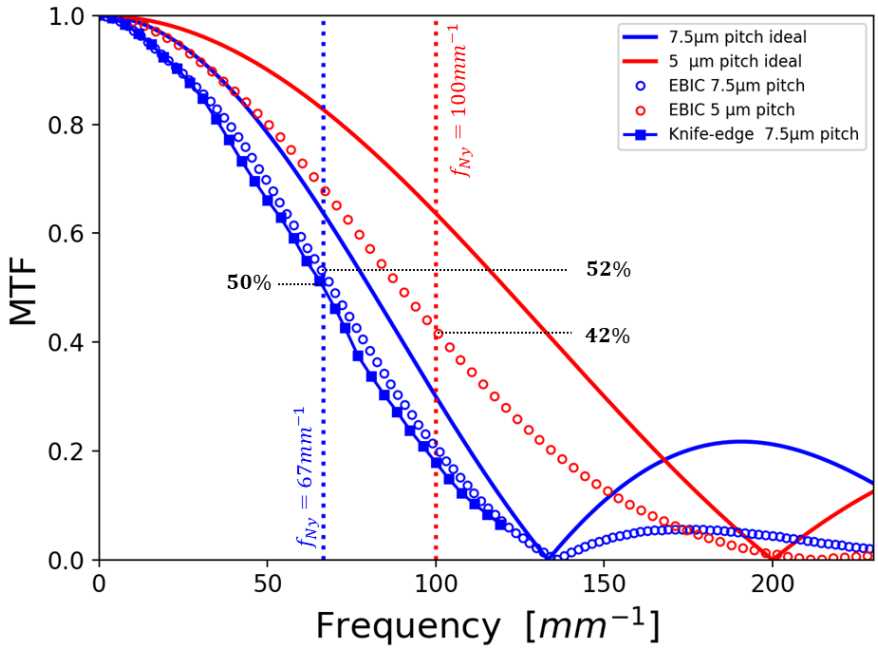

Figure 4. MTF estimation performed with 2D fast Fourier transform from PSF in Figure 2

EBIC measurements allow optimizing the development of the p/n technology, to get the optimal structure that favors the charge distribution between pixels. Figure 5 shows EBIC acquisitions performed on two optimized array diodes with 7.5µm and 5µm pixel pitch. Compared to the Figure 2, these PSF show an even more pronounced cloverleaf shape, highlighting a stronger self-confinement effect. In Fourier space, the corresponding MTF are closer to the ideal case. Indeed, the MTF at Nyquist are **56%** and **53%** respectively. These values, close to the ideal MTF (64%), demonstrate the progress of the development of the p/n technology with pixels much smaller than the diffusion length.

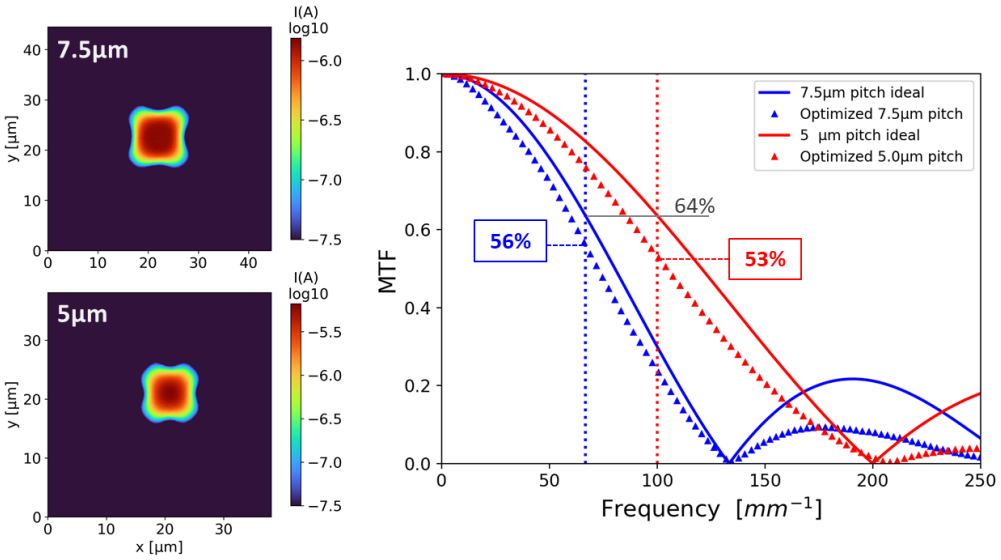

Figure 5 EBIC scans of optimized p/n array diodes of 7.5µm and 5µm pixel pitch (left). MTF estimation carried out with 2D fast Fourier transform from EBIC scans (right).

4. SIMULATION RESULTS

EBIC MTF estimation by Monte Carlo simulations

The interest of the EBIC technique is the resolution power of the SEM, limited by the interaction volume (carrier generation volume). The knowledge of the dimensions of this volume allows quantifying its convolution with the spatial response of the characterized pixel. In frequency space, it corresponds to the multiplication of the pixel MTF with the Fourier transform of this volume (EBIC MTF).

In this work, the generation volume is determined by Monte Carlo simulations through the CASINO software [7] [8]. This software allows the simulation of the interactions between the incident electrons and the MCT. At each inelastic interaction, incident electrons lose energy and change their trajectory until they are completely slowed down. At the end of the simulations, CASINO provides maps of the energy deposited in the active layer in the xy planes (normal planes to the beam) and in the xz planes (parallel planes to the beam). To find the minority carriers generated at each position, this energy is divided by the required energy to create an electron-hole pair given by the Price relation [9].

Then, the EBIC LSF is determined by integrating the generated carriers along the beam penetration depth (z) and along the direction of the normal plane of incidence of the beam (x or y). Thus, the LSF obtained from the Monte Carlo simulation of the interactions between 10^4 electrons accelerated to 15keV and the MCT is plotted in gray in Figure 6(a). Similarly, the LSF of the confined diodes determined previously is also plotted in order to highlight the thinness of the electron beam with respect to the dimensions of the analyzed diodes. Indeed, the profile of the spatial response of the EBIC has a FWHM estimated at 0.21µm, much narrow than the FWHM calculated for the characterized diodes of 7.5µm and 5µm pixel pitch: 7.41 and 5.15µm.

The Fourier transforms of these LSF are shown in Figure 6(b). The EBIC MTF introduces a degradation on the pixel experimental MTF. Therefore, at the 67mm^{-1} Nyquist frequency, the EBIC MTF is estimated to 99.83%, i.e., the MTF associated with 7.5µm pixel pitch is degraded by 0.17%. Similarly, for the 5µm pixel pitch, the EBIC MTF is 99.14% corresponding to a degradation of 0.86% on the real pixel MTF. These small degradations, less than 1%, on the EBIC MTF measurements of small pixel pitches can be neglected, demonstrating the direct measurement of the MTF without the need for deconvolution.

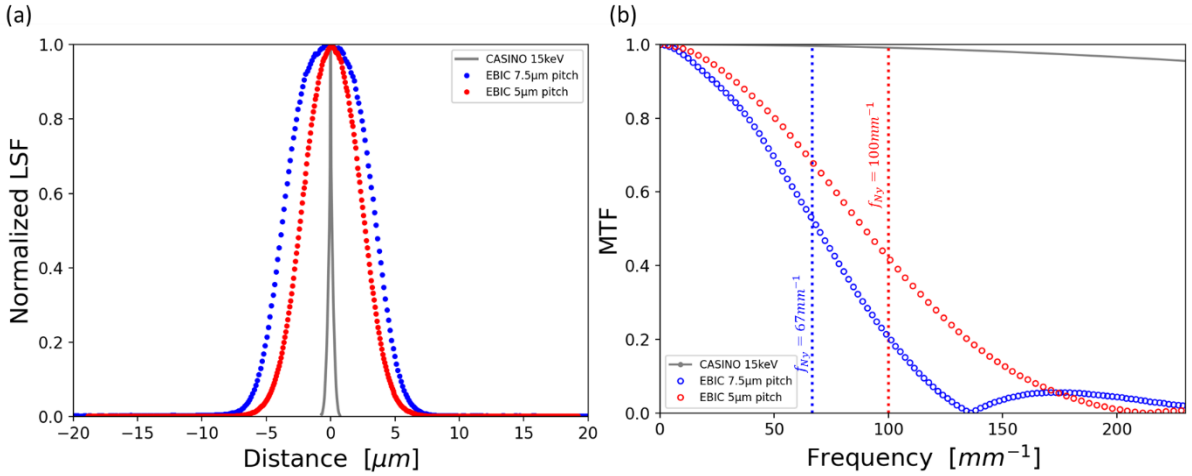

Figure 6. Comparison between EBIC spatial response and measured spatial responses of a 7.5µm and 5µm pitch array diodes in (a) real space and (b) Fourier space.

Depth carrier generation by an electron-beam

From the simulated interaction volume (image framed in red in the Figure 7), it is also possible to determine the generation profile in depth (along z) by integrating the carriers created along x and y. The resulting generation profile is shown in dotted line in Figure 7, it fits well with a modified Gaussian function written as follows:

$$G_{EBIC}(z) \propto e^{-\frac{(z-R_p)^2}{2(\sigma_0+\alpha z)^2}} \quad (2)$$

with R_p the depth where generation is maximum, σ_0 the variance and α a fitting coefficient. The values that fit well with the simulated profile are: $R_p = 0.12\mu m$, $\sigma_0 = 0.15\mu m$ and $\alpha = 0.12$.

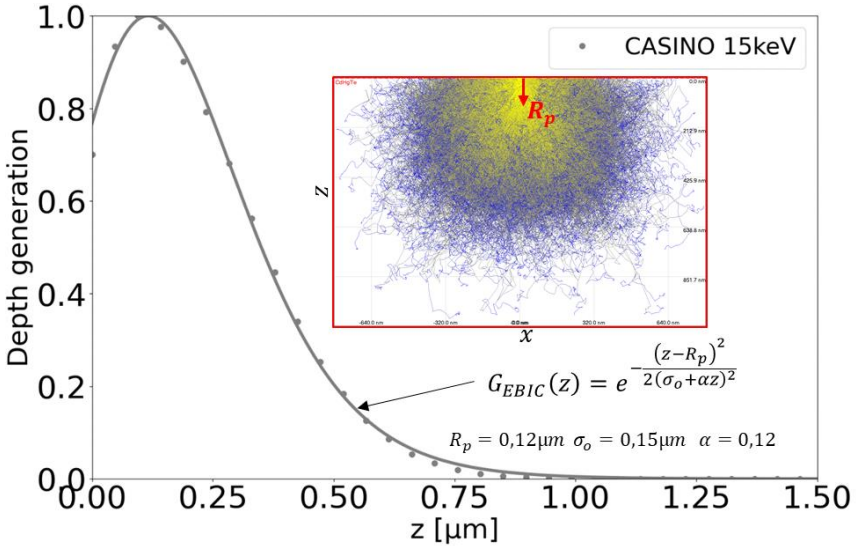

Figure 7. Normalized depth generation calculated from the interaction volume obtained by CASINO simulation of a 15keV energy beam in the MCT (image in red frame).

Comparison with MTF computed by finite-element modeling

The MTF obtained by the EBIC method are compared with finite element simulations performed with the FreeFem++ software [10]. This tool allows to solve the continuity equation in the diffusion zone, i.e., in the n-doped layer. In the stationary state and neglecting electric fields in the structure, the drift-diffusion equation is simplified by the ambipolar diffusion equation:

$$\frac{n}{L_d^2} + \vec{\nabla}\left[-\vec{\nabla}n\right] = G \tag{3}$$

with n the excess hole density, L_d the hole diffusion length and G the carrier generation in the active layer.

The carrier generation is not homogeneous in the material; it depends on the carrier generation profile in the MCT and the exposure profile at the incident surface $P(x,y)$. In the case of carrier generation by an electron beam, it was found by Monte Carlo simulations the equation (2) describing the electron generation profile in the MCT, $G_{EBIC}(z)$. Thus, the carrier generation in the n-doped MCT can be written as follows:

$$G(x,y,z) = P(x,y) \times e^{-\frac{(z-R_p)^2}{2(\sigma_0+\alpha z)^2}} \tag{4}$$

To simulate the carrier distribution directly in frequency space, the excitation profile $P(x,y)$ can be written as a cosine function containing the spatial frequency at which the MTF is determined:

$$P(x,f) = \frac{1}{2}[1 + \cos(2\pi f x)] \tag{5}$$

The differential equation is solved in 3D considering a simplified configuration as shown in Figure 8 where three pixels are represented. The boundary conditions applied are the same as in the references [5] [11]:

- At the junction, all minority carriers are collected: $n = 0$ (Dirichelet condition)
- Recombination of carriers at the surfaces: $\frac{\partial n}{\partial \vec{u}} = -S \times n$ with S the surface recombination velocity (Neuman condition).
- At lateral symmetries: $\frac{\partial n}{\partial \vec{u}} = 0$ (Neuman condition)

After solving the differential equation, the minority carrier density $n(x,y,z)$ is obtained at a certain spatial frequency f. The integral of the gradient of $n(x,y,z)$ gives $I(f)$, the total current through the junction. Then, the resulting current is compared to the current obtained without electronic excitation $I(0)$. Therefore, the MTF at frequency f is given by the relation:

$$MTF(f) = 2\frac{I(f)}{I(0)} - 1 \tag{6}$$

For example, the current calculated at the Nyquist frequency corresponds to the excitation profile shown in Figure 8, where the center diode (in red) is illuminated in the same way as a diode at a distance of $2 \times pitch$. To describe the entire MTF curve, it is necessary only to vary the frequency of the cosine excitation profile $P(x,f)$. In order to reduce the calculation time, it is possible to take into consideration the symmetries passing through the middle of the central diode ($x = 0$) and the middle of the first neighboring diode ($x = pitch$). To better describe the MTF at frequencies higher than the Nyquist Frequency, it is necessary to increase the domain of simulated diodes. The 3D simulations were performed on a domain of width $5 \times pitch$, going from the center of the central diode to the center of its fourth neighbor.

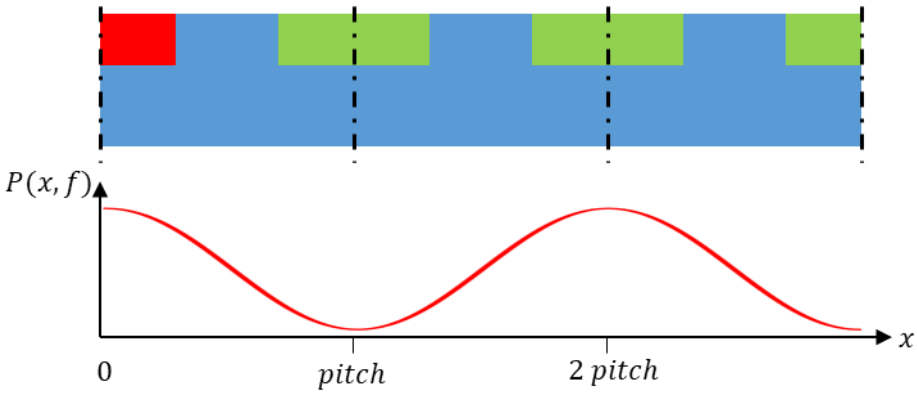

Figure 8. Illustration of simulated structure domain and associated Nyquist frequency excitation profile $P(x, f_{Ny})$

Using this computational procedure, the simulated MTF at different frequencies and for pixel pitches of 7.5 and 5µm are shown as blue and red triangles in Figure 9. In this figure, the MTF estimated from EBIC scans in Figure 2 are also represented by circles. The superposition of the curves corresponding to the simulations and the EBIC measurements show that the charge distribution between pixels can be well modeled by the diffusion of carriers in the active zone.

The MTF measurements performed in this work were done using electrons instead of photons. However, the photodiodes are designed to detect photons in the MWIR range. In fact, the cut-off wavelength of these diodes is about 5µm with the maximum response at 4µm. The question is therefore to know if these EBIC measurements describe the real case of diodes where they are illuminated by photons. In this regard, finite element simulations have also been performed but replacing the electronic generation profile $G_{EBIC}(z)$ by the photonic generation profile $G_{ph}(z)$ described by the Beer-Lambert law:

$$G_{ph}(z) \propto e^{-\alpha z} \tag{7}$$

with α the absorption coefficient.

Using the Moazzami relation [12], this coefficient is equal to 8130cm^{-1} in the case of photons of wavelength 4µm absorbed by n-doped MCT, corresponding to a penetration depth of $\alpha^{-1} = 1.23\mu m$. The resulting MTF are plotted with crosses in Figure 9. In the bandwidth, containing frequencies in the interval $[0, f_{Ny}]$, these curves show a very good accuracy between measured and simulated MTF using an electronic or photonic excitation. However, for frequencies above Nyquist, the MTF curves from the photon generation tend to decrease more rapidly and the first zero shifts to the left. This difference may be due to the fact that photons are absorbed in the entire volume of the structure, and not only close to the incidence surface as in the case of electrons. In this model, only the contribution of the diffusion in the active zone is taken into account, neglecting the contribution of the depletion region. In the case of photogeneration, a non-negligible amount of carriers is photogenerated directly in the depletion region because the photons are absorbed in the whole MCT volume. To improve the model, it will therefore be necessary to add the contribution of the depletion region and study its impact on the high frequencies. In addition, in the case of photon generation, a second generation term was taken into account due to the reflection of photons by the metal contacts on the front surface.

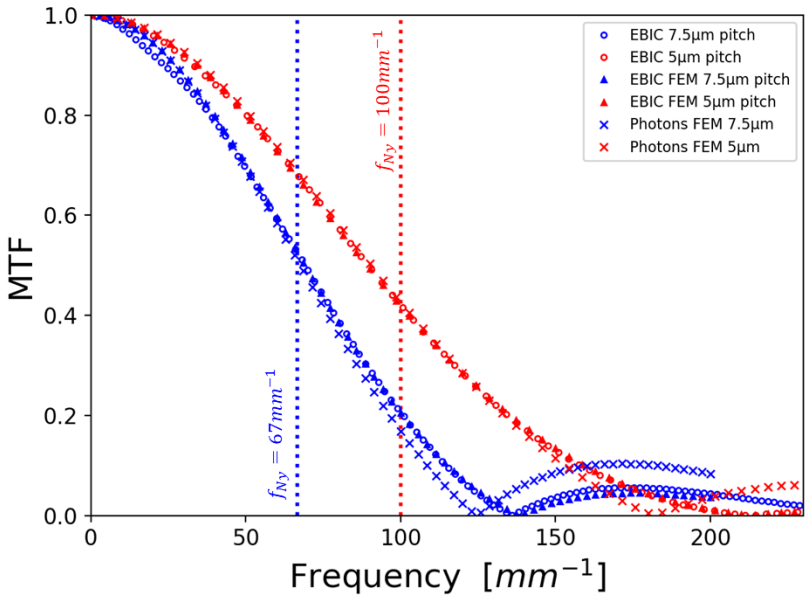

Figure 9. Comparison between MTF measurements by EBIC and MTF computing by FEM for an electronic and photonic generation.

5. CONCLUSION

This work presented spatial response measurements obtained by the EBIC method. Two diode mini-arrays of 7.5µm and 5µm pixel pitch have been compared in terms of FWHM and MTF. In real space, the FWHM extracted from the measured PSF are 7.41 and 5.15µm respectively. Even using a planar structure, we therefore manage to mitigate lateral diffusion decreasing the pixel pitch to values much smaller than the minority carrier diffusion length. In Fourier space, the pixel pitch reduction shows an improvement of the MTF at all frequencies and the bandwidth limited by the f_{Ny} is increased. At Nyquist, the extracted MTF are 52% and 42% respectively. The 7.5µm pixel MTF is closer to the ideal case having a 64% MTF at Nyquist. By the classical optical knife-edge method, we also confirmed this high MTF estimated equal to 50% for a FPA containing diodes of the same structure as those characterized by EBIC.

In contrast to optical projection methods, the measurement of MTF by EBIC is direct because the degradation introduced by this method estimated by Monte Carlo simulations is lower than 1%, hence it can be neglected. Comparison between experimental and modelling MTF demonstrated the accuracy of EBIC technique in the estimation of small pixel IR detector MTF in the frequency bandwidth $[0, f_{Ny}]$. Above Nyquist frequency, further studies are needed to understand the difference between MTF obtained from electronic and photonic excitations.

Being an effective technique, EBIC allowed us to characterize several technological variants and find the best configuration to optimize the MTF. Thus, optimized array diodes of 7.5µm and 5µm have reached an MTF on **56%** and **53%** at Nyquist (see Figure 5), demonstrating the progress of the new generation p/n technology.

REFERENCES

[1] O. Gravrand *et al.*, "Design of a small pitch (7.5µm) MWIR HgCdTe array operating at high temperature (130K) with high imaging performances," in *Infrared Technology and Applications XLVIII*, G. F. Fulop, M. Kimata, L. Zheng, B. F. Andresen, J. L. Miller, and Y.-H. Kim, Eds., Orlando, United States: SPIE, May 2022, p. 26. doi: 10.1117/12.2618852.

[2] R. G. Driggers, "Infrared detector size: how low should you go?," *Opt. Eng*, vol. 51, no. 6, p. 063202, Jun. 2012, doi: 10.1117/1.OE.51.6.063202.

[3] A. Yèche *et al.*, "MTF Characterization of Small Pixel Pitch IR Cooled Photodiodes Using EBIC," *Journal of Electronic Materials*, vol. 49, no. 11, pp. 6900–6907, 2020, doi: 10.1007/s11664-020-08253-0.

[4] A. Yèche, F. Boulard, and O. Gravrand, "Development of Electron Beam Induced Current Characterization of HgCdTe Based Photodiodes," *Journal of Elec Materi*, vol. 48, no. 10, pp. 6045–6052, Oct. 2019, doi: 10.1007/s11664-019-07140-7.

[5] O. Gravrand, J. C. Desplanches, C. D. Gue, G. Mathieu, and J. Rothman, "Study of the Spatial Response of Reduced Pitch Hg1ÿxCdxTe Dual-Band Detector Arrays," p. 7, 2006.

[6] I. A. Cunningham and A. Fenster, "A method for modulation transfer function determination from edge profiles with correction for finite element differentiation," *Medical Physics*, vol. 14, no. 4, pp. 533–537, 1987, doi: 10.1118/1.596064.

[7] D. Drouin, P. Hovington, and R. Gauvin, "CASINO: A new monte carlo code in C language for electron beam interactions—part II: Tabulated values of the mott cross section," *Scanning*, vol. 19, no. 1, pp. 20–28, 1997, doi: 10.1002/sca.4950190103.

[8] D. Drouin, A. R. Couture, D. Joly, X. Tastet, V. Aimez, and R. Gauvin, "CASINO V2.42—A Fast and Easy-to-use Modeling Tool for Scanning Electron Microscopy and Microanalysis Users," *Scanning*, vol. 29, no. 3, pp. 92–101, 2007, doi: 10.1002/sca.20000.

[9] S. L. Price, "Electron-beam induced current measurement of HgCdTe heterojunction infrared detectors," in *1984 International Electron Devices Meeting*, IRE, 1984, pp. 560–563. doi: 10.1109/IEDM.1984.190781.

[10] FreeFEM software. Available: https://freefem.org/

[11] O. Gravrand *et al.*, "MTF study of planar small pixel pitch quantum IR detectors," presented at the SPIE Defense + Security, Baltimore, Maryland, USA, B. F. Andresen, G. F. Fulop, C. M. Hanson, and P. R. Norton, Eds., Baltimore, Maryland, USA, Jun. 2014, p. 12. doi: 10.1117/12.2053874.

[12] K. Moazzami *et al.*, "Detailed study of above bandgap optical absorption in HgCdTe," *Journal of Elec Materi*, vol. 34, no. 6, pp. 773–778, Jun. 2005, doi: 10.1007/s11664-005-0019-3.